Liquid Crystals
Publication details, including instructions for authors and subscription information:
http://www.informaworld.com/smpp/title~content=t713926090

Polymerization-induced phase separation III. Morphologies and contrast ratios of polymer dispersed liquid crystals

C. Serbutoviez; J. G. Kloosterboer; H. M. J. Boots; F. A. M. A. Paulissen; F. J. Touwslager

Online publication date: 06 August 2010

To cite this Article Serbutoviez, C. , Kloosterboer, J. G. , Boots, H. M. J. , Paulissen, F. A. M. A. and Touwslager, F. J.(1997) 'Polymerization-induced phase separation III. Morphologies and contrast ratios of polymer dispersed liquid crystals', Liquid Crystals, 22: 2, 145 — 156
To link to this Article: DOI: 10.1080/026782997209504
URL: http://dx.doi.org/10.1080/026782997209504

LIQUID CRYSTALS, 1997, VOL. 22, NO. 2, 145–156

Polymerization-induced phase separation III. Morphologies and contrast ratios of polymer dispersed liquid crystals†

by C. SERBUTOVIEZ‡, J. G. KLOOSTERBOER*, H. M. J. BOOTS, F. A. M. A. PAULISSEN and F. J. TOUWSLAGER

Philips Research Laboratories, Professor Holstlaan 4, 5656 AA Eindhoven, The Netherlands

(*Received 10 June 1996; accepted 23 August 1996*)

Polymerization induced phase separation in mixtures of liquid crystals (LCs) and acrylates (Merck TL205/PN393) proceeds by liquid–gel demixing, in most cases of practical interest. At high LC content or low temperature of polymerization liquid–liquid separation cannot be excluded. Depending on the elasticity and homogeneity of the polymer network at the onset of phase separation, spherical or non-spherical LC domains are observed; non-spherical domains reflect an inhomogeneous gel structure. The change from spherical to non-spherical occurs in a very narrow range of LC concentrations and curing temperatures. The transition between these two morphologies can be explained using conversion phase diagrams obtained from the Flory–Huggins–Dušek theory. The contrast ratio of PDLCs made from the Merck mixture passes through a maximum when the droplet shape at the onset of phase separation changes from spherical to non-spherical. Lowering the LC content or increasing the temperature leads to smaller LC domains which scatter less efficiently. The reverse changes lead to early phase separation and large LC domains which also scatter inefficiently. It is speculated that the maximum of the contrast ratio is related to secondary phase separation, leading to subdomains of an appropriate size.

1. Introduction

Polymer Dispersed Liquid Crystal (PDLC) materials are promising materials for the preparation of electro-optical devices such as displays and electrically controllable light shutters [1–4]. UV light-induced polymerization is presently the most common technique for making PDLCs. It is well-known that the electro-optical performance of PDLCs depends on a large number of parameters such as type and concentration of LC, type and functionality of monomers, UV intensity, temperature of polymerization, crosslink density, etc. [1, 4–8]. Rather than studying many different systems and changing many parameters, we have recently analysed the phase separation process in a model system composed of a single LC compound and a single monomer [9]. It emerged that liquid–gel phase separation occurs rather than liquid–liquid demixing. We also found that either spherical or non-spherical nematic liquid crystal domains appear at the onset of phase separation, depending on the structure and the amount of polymer gel at the appearance of the nematic phase.

Using the concept of a conversion phase diagram, predictions of morphology can be made in a qualitative way [10]. The next step would be to relate these morphological changes to the electro-optical performance of PDLCs. However, this was impeded by the poor contrast ratio, high switching voltage and strong hysteresis of PDLCs made from the simple model system. Therefore, we have switched to PDLCs made from a well-known and widely used commercially available mixture, TL205/PN393. TL205 is an LC mixture containing halogenated biphenyl and terphenyl compounds; PN393 is a mixture of mono- and multi-functional acrylates. Although this is a multicomponent system, we will treat it as a pseudo-ternary system composed of monomer (M), LC solvent (LC), and polymer (P). We will first report the phase diagram of the unpolymerized starting mixture, then explain the differences in morphology obtained under various polymerization conditions using conversion phase diagrams, and finally we will relate these differences to variations of the contrast ratio.

A clear relationship will be shown to exist between the values of the contrast ratio and the size and the

*Author for correspondence.

† II: ref. 9. I: ref. 10.

‡ Present address: Thomson LCD, Sextant Avionique, Z.I. Centr.Alp., 38430 Moirans, France.

0267–8292/97 $12·00

shape of the liquid crystal domains at the onset of phase separation. Its existence will be rationalized on the basis of the conversion-phase diagram which also guides in choosing the proper reaction conditions to obtain the desired morphology.

2. Experimental

2.1. *Chemicals*

TL205 and PN393 were obtained from Merck Ltd (Poole, UK). The physical characteristics of TL205 are the following: $T_{N\rightarrow I}=87{\cdot}4°C$, $\Delta n=0{\cdot}2175$, $\Delta\varepsilon=5{\cdot}0$.

2.2. *Phase diagram before polymerization*

The phase diagram of the model system PN393/TL205 was determined by microscopy. Various mixtures were heated above their clearing temperature, then one drop was sandwiched between two glass plates containing glass fibre spacers with a thickness of 18 μm, and next the samples were mounted on the heating/cooling stage (Linkam TMS 92/THMS 600) of a polarizing microscope. The light from the lamp of the microscope was filtered with a Kapton foil to avoid unwanted exposure to UV. The sample was heated above its clearing point and then cooled and observed under the microscope while cooling to −40°C; it was then heated back to its clearing point. Heating and cooling rates were varied between 10 and 5°C min^{-1} during each scan, the lowest rate being used near the phase transition.

2.3. *Photopolymerization under the microscope*

The samples were prepared in the same way as those used for the determination of the phase diagram. They were cured by radiation from a high pressure mercury lamp equipped with an optical fibre (Efos Ultracure 100). The UV intensities were measured at the sample surface at a wavelength of 365 nm. UV intensities were generally low (0·1–1 mW cm^{-2}) in order to bring the rate of phase separation into an easily accessible time domain. The UV irradiation was stopped at the onset of the phase separation and the behaviour of the droplets was examined. The samples were then cooled down at 1 °C min^{-1} during 5 minutes and then heated back to their original curing temperature. When phase separation sets in during polymerization, a front-like formation of droplets occurs due to the unavoidable intensity gradient in our set-up. Observations were made using a standard magnification of 200×. The resolution on the video screen was then about 1 μm. In a few cases, a high speed video recording was made during exposure at 7 mW cm^{-2} (Kodak Ektapro EM). The sampling rate was 500 frames s^{-1}. The high speed camera reduced the resolution to about 1·5 μm. At the sampling rate chosen, the time interval of observation was about 3 s.

2.4. *Photopolymerization in the DSC*

Samples were made by sandwiching a droplet between a polished silicon disc and a glass disc of 7 mm diameter. Spacers of 18 μm were used for thickness control. Light intensities were varied between 0·07 and 7 mW cm^{-2}. The DSC measures the exothermic heat flux of the polymerization reaction which is proportional to the rate of reaction. Integration yields the heat of reaction, and division by the total heat of reaction gives the double bond conversion, assuming total conversion at the end of the reaction. The DSC had been modified to monitor the intensity of a HeNe laser beam reflected at the bottom of the sample. When the sample becomes turbid due to nematic phase formation the intensity of the reflected light beam drops considerably. The DSC curve enables calculation of the conversion at which turbidity sets in. The formation of isotropic droplets cannot be observed with the thin samples used. Further details have been given elsewhere [11, 12].

2.5. *Electro-optical measurements*

The measurements for electro-optical characterization of PDLC cells were performed on a modified Display Measuring System (DMS) from Autronic GmbH (Karlsruhe, Germany). The cells were illuminated by a narrow white light beam with a divergence of 1·5°. The full collection angle was 5·2°. Detection and measurement of the intensity of transmitted light was made with a photomultiplier. Addressing was achieved with a square wave ($f=1$ kHz) and the voltage increase as a function of time was 0·05 V s^{-1}. All measurements were performed at room temperature.

3. Results

3.1. *Binary phase diagram before polymerization*

The phases observed upon cooling and heating mixtures of TL205 and PN393 are depicted in figure 1. The general shapes of the two diagrams are similar; however, the phase transition curves obtained on cooling are shifted to lower temperatures due to supercooling (dashed areas). Two single phases, isotropic (I) and nematic (N), and one large biphasic region (I + N) can be identified. No crystallization was observed in the range of temperatures and concentrations studied.

Figure 2 shows a microscope picture of a mixture containing 80 wt % of TL205 and 20 wt % of PN393 at −5°C between crossed polarizers. Thermal phase separation has led to the formation of a two phase system composed of a dispersion of nearly equally sized LC droplets (around 15 μm) in an isotropic liquid. If such a dispersion could be stabilized by polymerization, PDLCs with a low polydispersity in LC domain size would be obtained. However, polymerization leads to the formation of many new, small domains (see § 3.2.1).

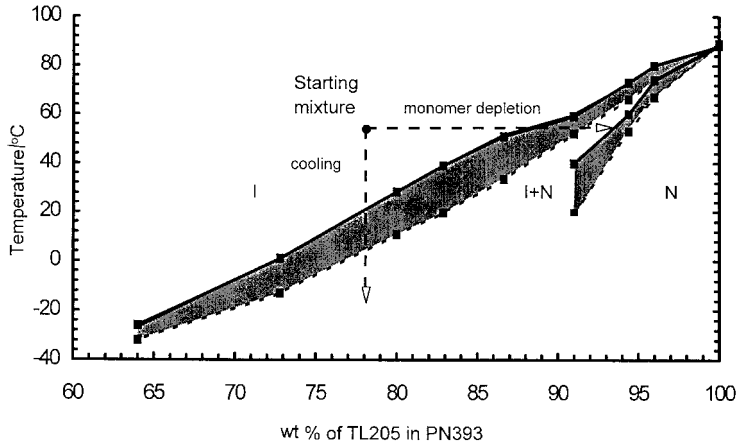

Figure 1. Phase behaviour of the technical system TL205/PN393 observed upon cooling (dashed line) and upon heating (continuous line). I: isotropic phase; N: nematic phase. Upper hatched area: supercooled isotropic liquid; lower hatched area: supercooled nematic phase. Dotted arrows depict the isothermal and isoconcentration modes of phase separation.

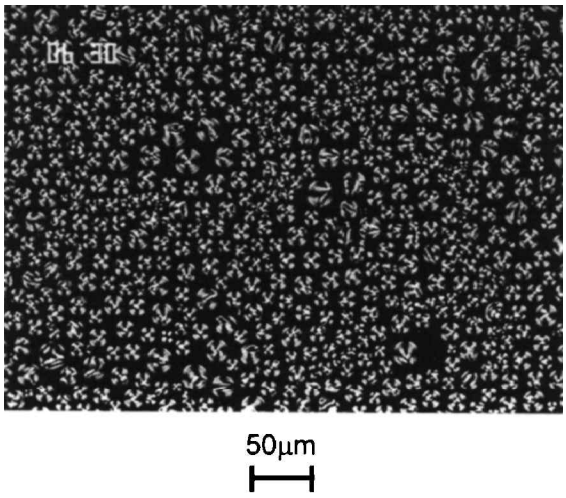

Figure 2. Unpolymerized mixture containing 80 wt % of TL205 and 20 wt % of PN393, cooled from +40 to −5°C. Crossed polarizers.

3.2. *Polymerization-induced phase separation and morphology*

The onset of phase separation shows up as a front-like formation of droplets due to the unavoidable intensity gradient under our microscope. The droplets are nematic as soon as they appear. For clarity, pictures have been taken mainly near this front. Further in the sample or later in time, the droplet density increases considerably. Depending on the LC content and the reaction temperature, coalescence does or does not occur. In the limited resolution depth of our microscope, a spaghetti-like structure develops during continued exposure. Pictures of that structure are less informative than the ones obtained near the front. We were unable to determine whether or not co-continuous phases were formed in the final stage. If coalescence occurs it shows up on the video. We have studied the influence of LC content and temperature of polymerization on the morphology. We have also determined the conversion at incipient phase separation.

3.2.1. *Variation of LC concentration and temperature*

In order to investigate the influence of the polymer network on the morphology of PDLCs, we have monitored the photopolymerization of the technical system at high, intermediate and low concentrations of TL205 and at different curing temperatures. The observations during polymerization and subsequent cooling and heating are summarized in table 1. In the first series, concentrations ranged from 83 to 96 wt % of TL205 (table 1, samples 1 to 3). In order to start the photopolymerization in the isotropic state, the first two samples had to be heated to 75 and 60°C, respectively. Sample 3 was isotropic at 25°C (cf. figure 1). The samples polymerized at high temperature required a high UV dose for phase separation to start (cf. samples 1 and 2 with sample 3). At the onset of the phase separation, only a few nematic droplets were present and pronounced coalescence was observed. By contrast, the phase separation in sample 3 already occurred after a UV dose of 69 mJ cm^{-2}. Large numbers of droplets were formed, all of them spherical and nematic with sizes ranging from 10 to 25 μm. Since the cell gap used was 18 μm, the larger domains extend from the top to the bottom of the cell. As in the former cases, significant coalescence was observed. Resumption of the irradiation in sample 3 caused the formation of new domains and further coalescence. Subsequent cooling led to an increase of the size of the existing LC droplets and only very few new LC droplets were formed. By heating the sample back to its curing temperature, the size of the small droplets decreased, and at 25°C only a few large droplets remained. A permanent change in morphology had occurred.

In the second series of experiments, the LC concentrations ranged from 76 to 81 wt % (table 1, samples 4–8). In sample 4 (figure 3), small spherical nematic droplets

Table 1. Microscopic observations during polymerization-induced phase separation in TL205/PN393.

Sample no. (figure no.)	LC content/ wt % TL205	Curing temp./°C	UV intensity/ mW cm^{-2}	Irradiation time to phase sepn./s	Dose/ mJ cm^{-2}	Droplet shape
	High					
1	96	75	0·3	625	187	spherical and nematic
2	90	60	0·6	290	174	spherical and nematic
3	83	25	0·3	232	69	spherical and nematic
	Medium					
4 (3)	81	25	0·3	297	89	spherical and nematic
5 (4)	80	25	0·3	317	95	non-spherical and nematic
6 (5)	80	20	0·3	148	44	spherical and nematic
7 (6(*a*))	80	40	0·3	491	147	non-spherical and nematic (v. small)
8	76	25	0·3	514	163	non-spherical and nematic (v. small)
	Low					
9, 10	72–70	25	0·6–6	—	—	extremely small nematic domains
11–13	65–40	25	0·6–6	—	—	no visible phase separation

Sample no. (figure no.)	Coalescence during exposure	Second exposure (few s, same UV intensity)	Effect of cooling to 5°C below T_{cure} at 1°C min^{-1}	Effect of reheat to T_{cure} at 1°C min^{-1}
1	yes	—	—	—
2	yes	—	—	—
3	yes (large polydispersity in size)	formation of new domains; increased coalescence	increase of droplet size; no new droplets	decrease of LC domain size; at 25°C few large droplets; permanent change in morphology
4 (3)	hardly any	LC depletion zone between new and first formed droplets	slight increase of droplet size; new spherical droplets	decrease of droplet size; recovery of original morphology
5 (4)	no	—	slight increase of droplet size; new deformed LC domains	decrease of droplet size; nearly full recovery of original morphology
6 (5)	yes	—	increase of droplet size; new droplets	decrease of droplet size; partial change in morphology
7 ((6*a*))	no	—	—	—
8	no	—	—	—
9, 10	not observable	—	—	—
11–13	not observable	—	—	—

—: not done or not determined.

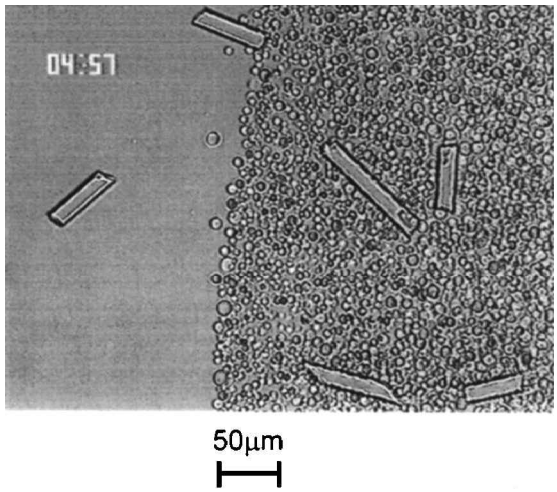

Figure 3. Spherical nematic droplets at the onset of phase separation. Composition: 81 wt % of TL205, 19 wt % of PN393; temperature: 25°C; $I_{UV}=0{\cdot}3\,mW\,cm^{-2}$; irradiation time: 297 s. Straight bars are glass spacers with a thickness of 18 μm. No polarizers.

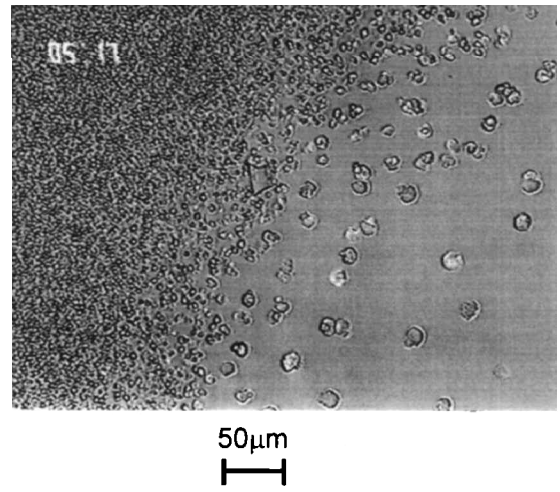

Figure 4. Non-spherical nematic droplets at the onset of phase separation. Composition: 80 wt % of TL205, 20 wt % of PN393; temperature: 25°C; $I_{UV}=0{\cdot}3\,mW\,cm^{-2}$; irradiation time: 317 s. Straight bars are glass spacers with a thickness of 18 μm. No polarizers.

phase separated after a UV dose of $87\,mJ\,cm^{-2}$ (figure 3). Very few coalescence events were observed, most of the droplets remaining separated. Resumption of the irradiation (second exposure in table 1) led to a depletion zone around existing domains. This shows that at the onset of the second phase separation, the system was far from equilibrium. Cooling from 25 to 20°C led to the formation of new spherical nematic droplets all over the sample. During subsequent heating, droplets which were formed during cooling disappeared again.

At 80 wt % TL205, the phase separation occurred somewhat later, after a UV dose of $95\,mJ\,cm^{-2}$ (sample 5). The LC phase nucleated as spherical, nematic droplets, but as these expanded their size, their shape rapidly became non-spherical (figure 4). No coalescence was observed in this system and, upon cooling, not only the size of the existing non-spherical droplets increased, but also many new, large, deformed LC domains were formed all over the sample. During subsequent heating, most of the droplets which had been formed during cooling disappeared again.

At 80 wt % TL205, a high speed video recording was also made at ambient temperature during exposure at $7\,mW\,cm^{-2}$. No significant differences from the regular speed recordings at 25°C were noticed; in particular no coalescence was observed. Unlike the other experiments, exposure was continued after phase separation set in.

If the UV-polymerization was performed at the same concentration, but at a temperature of 20°C (sample 6), spherical nematic droplets were formed at the onset of the phase separation (figure 5). Pronounced coalescence was observed in this sample. Upon cooling and heating, the droplets behaved in an intermediate way to those obtained in samples 3 and 4.

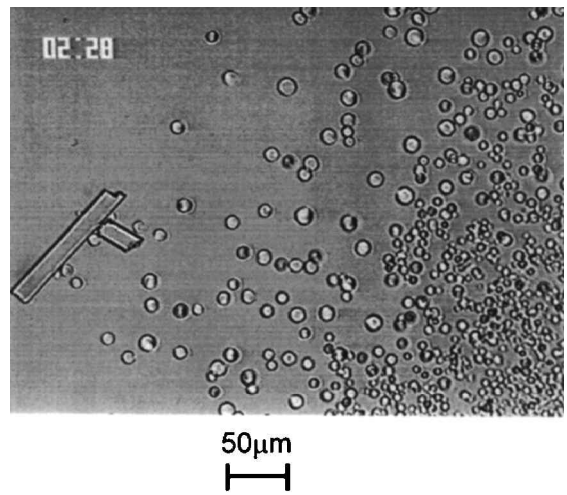

Figure 5. Spherical nematic droplets at the onset of phase separation. Composition: 80 wt % of TL205, 20 wt % of PN393; temperature: 20°C; $I_{UV}=0{\cdot}3\,mW\,cm^{-2}$; irradiation time: 148 s. Straight bars are glass spacers with a thickness of 18 μm. No polarizers.

At a curing temperature of 40°C (sample 7), the phase separation occurred after an exposure dose of $147\,mJ\,cm^{-2}$ and led to very small nematic and non-spherical domains with a size close to the limit of the resolution of the optical microscope (around 1 μm, figure 6 (*a*)). No coalescence was observed in this sample. A similar morphology could be obtained by polymerizing a mixture of 76 wt % of TL205 at 25°C (sample 8, figure 6 (*b*)).

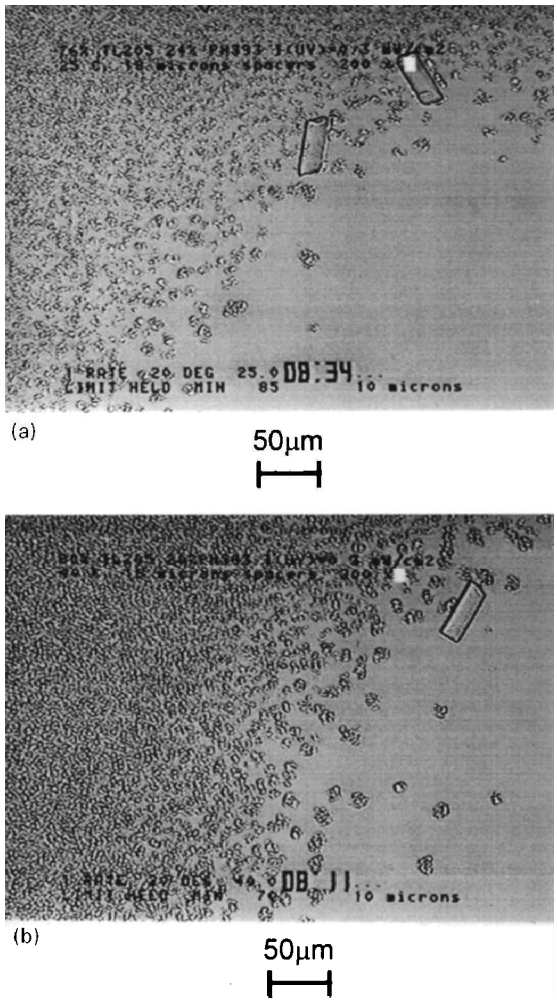

Figure 6. LC domains at the onset of phase separation. (*a*) Composition: 80 wt % of TL205, 20 wt % of PN393; temperature: 40°C; $I_{UV}=0{\cdot}3\,mW\,cm^{-2}$; irradiation time: 491 s. (*b*) Composition: 76 wt % of TL205, 24 wt % of PN393; temperature: 25°C; $I_{UV}=0{\cdot}3\,mW\,cm^{-2}$; irradiation time: 514 s. Straight bars are glass spacers with a thickness of 18 μm. No polarizers.

A third series of samples containing 40 to 72 wt % of TL205 was polymerized at 25°C (table 1). As in the case of the model system K15/TEGDA, the phase separation process was strongly delayed and the droplet size at the onset of the phase separation decreased as the LC concentration decreased (samples 9, 10) [9]. For concentrations below 70 wt % of TL205, no visible phase separation occurred under the microscope (samples 11–13). However, with crossed polarizers, some vague anisotropic patterns could be seen.

3.2.2. *Conversion at incipient turbidity*

The UV dose required for phase separation strongly depends on LC content and temperature (table 1). In order to check whether this is due to a difference in reaction rate or to a difference in conversion, we have simultaneously carried out photo-DSC and turbidity measurements. This technique allows the determination of the extent of double bond conversion at incipient turbidity, assuming total conversion at the end of the polymerization. It was checked with FTIR spectroscopy that the polymerization reaction indeed runs to completion. After 5 min of exposure at $7\,mW\,cm^{-2}$, the double bond conversion was >98%. A sudden increase of turbidity sets in at the appearance of a nematic phase. In the experiments described in § 3.2.1, the phase separated droplets were always nematic. Three different systems were measured, and results are shown in figures 7 and 8 and table 2.

In experiment 1 (figure 7), the phase separation occurred at 11% double bond conversion. This means that at the onset of the phase separation, the gel is loosely crosslinked (cf. sample 4 in table 1; however, in the DSC a higher light intensity was used throughout the series). In such a gel, spherical droplets are formed. In experiment 2 (figure 8), 22% of the double bonds had reacted at incipient turbidity. This showed up as a much later development of turbidity (cf. sample 5 in table 1). Non-spherical droplets were observed. In experiment 3, the decrease of LC concentration was compensated by the decrease of curing temperature. Phase separation started at 10% conversion. At this low gel content spherical droplets appeared (cf. sample 6 in table 1).

3.3. *Morphology at phase separation and contrast ratio*

Two series of PDLC cells were prepared. In the first series, the curing temperature was kept constant at 25°C and the percentage of TL205 in PN393 in the starting mixture was varied from 82 to 78 wt %. In the second series, a mixture containing 80 wt % of TL205 and 20 wt % of PN393 was polymerized at different temper-

Table 2. Double bond conversion at incipient turbidity; light intensity: $7\,mW\,cm^{-2}$.

Experiment no.	Composition wt % TL205/PN393	*T* °C	Conversion at turbidity/%	Droplet shape
1	81/19	25	11	spherical
2	80/20	25	22	non-spherical
3	80/20	20	10	spherical

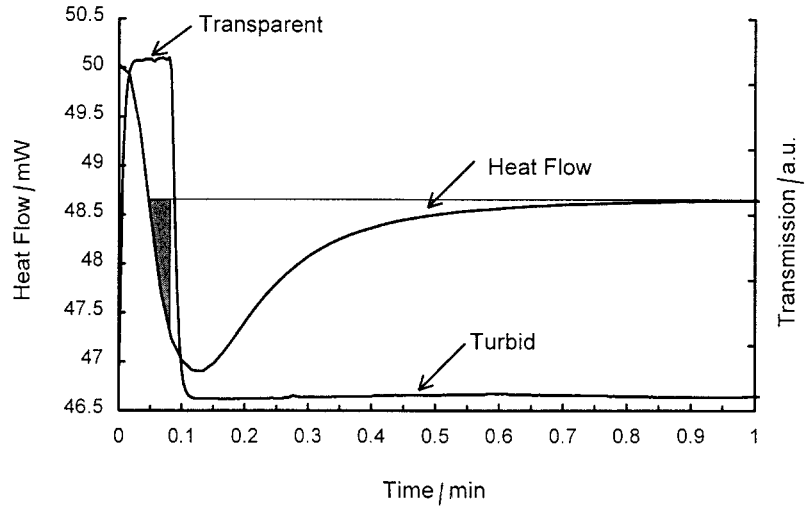

Figure 7. Photo-DSC/turbidity measurement: 81 wt% of TL205/19 wt% of PN393, cured at 25°C. I_{UV}= 7 mW cm^{-2}; C=C conversion at phase separation: 11%.

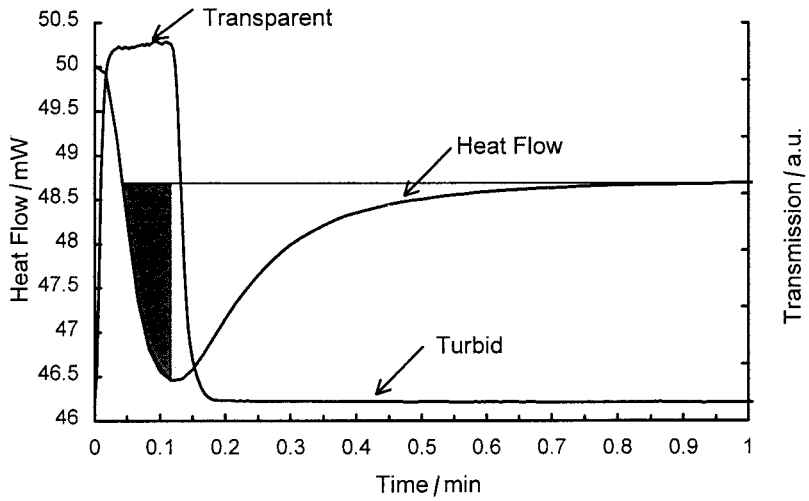

Figure 8. Photo-DSC/turbidity measurement: 80 wt% of TL205/20 wt% of PN393, cured at 25°C. I_{UV}= 7 mW cm^{-2}. C=C conversion at phase separation: 22%.

atures (from 15 to 60°C). The values of the contrast ratio (T_{on}/T_{off}) of these PDLC cells are plotted as a function of the polymerization conditions in figures 9 and 10. In figure 9 the contrast ratio increases strongly from 50 to 220 upon reduction of the LC content from 82 to 80 wt%. This steep transition occurs simultaneously with a change in shape of the LC droplets from spherical to non-spherical. When the LC concentration is further reduced, the contrast ratio decreases again. The influence of the curing temperature on the contrast ratio is shown in figure 10. The graph shows that the contrast ratio increases considerably when the temperature of polymerization is increased from 15 to 25°C. As in the first series of experiments, a significant increase of the contrast coincides with a change in shape of the domains from spherical to non-spherical. Figure 10 also shows that the contrast ratio decreases again when the temperature of photopolymerization is raised above 35°C.

4. Discussion

4.1. *Phase diagrams*

4.1.1. *Binary phase diagram of the LC–monomer mixture*

Before studying polymerization-induced phase separation, the phase behaviour of the unpolymerized model system should be established since it gives the thermodynamic stability of the starting mixture as a function of temperature and composition.

Although the system TL205/PN393 is a multicomponent system, we will consider it as a pseudo-binary system, assuming that the LC and the acrylate mixtures behave as pure components. However, the absence of crystallization in the temperature interval studied reflects the fact

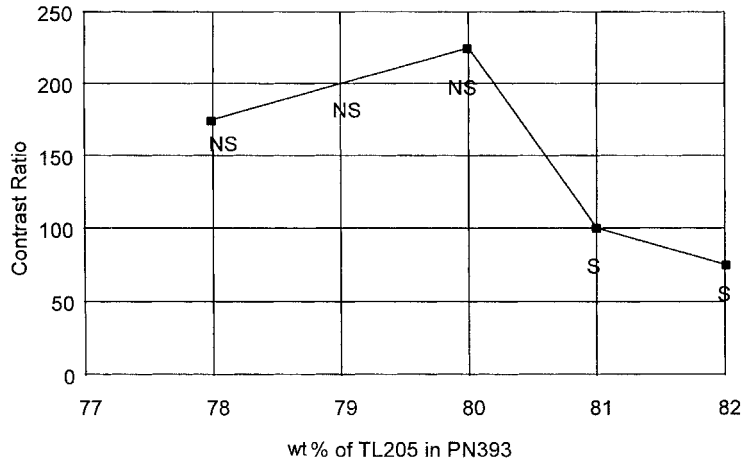

Figure 9. Contrast ratio as a function of the starting composition of the mixture TL205/PN393. Curing temperature: 25°C. $I_{UV}=7\,mW\,cm^{-2}$; irradiation time: 300 s. Shape of the LC domains at the onset of the phase separation: S=spherical droplets; NS=non-spherical droplets.

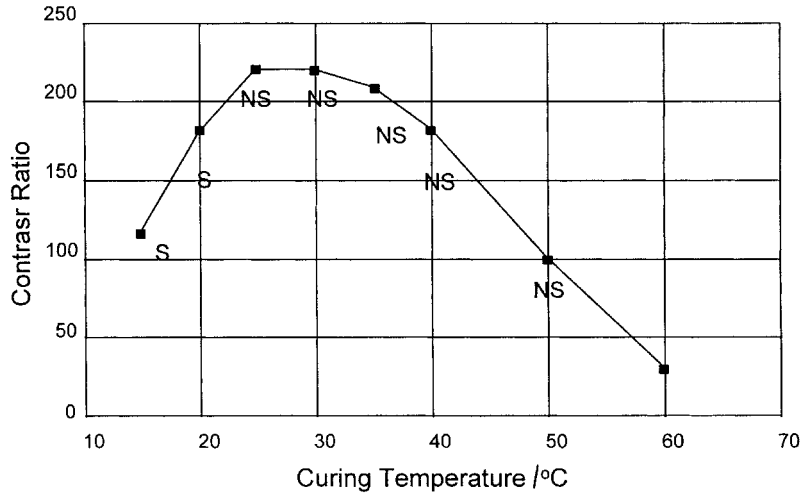

Figure 10. Contrast ratio as function of the curing temperature. 80 wt % of TL205/20 wt % of PN393. $I_{UV}=7\,mW\,cm^{-2}$; irradiation time: 300 s. Shape of the LC domains at the onset of the phase separation: S=spherical droplets; NS=non-spherical droplets.

that TL205 and PN393 are complex mixtures. The LC mixture has been deliberately designed to avoid crystallization near the intended temperature of use. Figure 1 shows that near the LC concentrations of practical interest (around 80 wt %), metastable solutions are easily obtained at ambient temperature.

Few binary phase diagrams of LCs and monomers have been reported in the literature. The phase diagram of the E7/NOA system has been reported by Smith [13], and the mixture of E8 and 2-ethylhexyl acrylate/urethane-diacrylate as prepolymer mixture has been reported by Hirai *et al.* [14]. Both are multicomponent systems. At a certain monomer/oligomer ratio, the system of Hirai *et al.* shows a liquid–liquid demixing curve with a clearly visible upper critical solution temperature (UCST). This curve overlaps with the nematic–isotropic transition range of the LC rich phase. Thus, their system differs from TL205/ PN393 and E7/NOA in indicating that demixing into two isotropic liquids must be possible. Hirai *et al.* did not however describe whether these two isotropic phases have indeed been observed. In the absence of the oligomer no UCST was observed.

4.1.2. *Phase diagrams and polymerization: conversion phase diagrams*

As mentioned in the Introduction, polymerization-induced phase separation in the K15/TEGDA model system proceeds predominantly through liquid–gel separation [9]. The absence of coalescence in many experiments with TL202/PN393 also points to liquid–gel phase separation. This process can be depicted in a ternary conversion phase diagram (figure 11). Along the M–LC and P–LC axes, concentrations are plotted in the conventional way, but along the M–P axis, the monomer conversion α is plotted. The polymerization of any LC–monomer mixture is represented by a horizontal arrow. The bold curved line shows the onset of the phase separation as a function of the initial composition of the LC–monomer mixture. An estimation of its

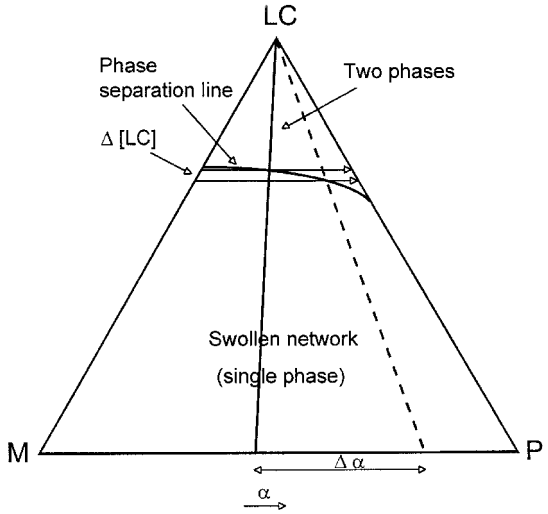

Figure 11. Ternary conversion phase diagram (schematic): effect of the initial composition on the phase separation process. α = degree of monomer conversion.

position can be obtained on the basis of the Flory–Huggins–Dušek theory and by making further assumptions about the respective χ values (χ_{M-LC}, χ_{M-P}, χ_{LC-P}) and the crosslink efficiency during polymerization [10]. Phase separation starts at the intersection of a polymerization line with the phase separation line. In figure 11, the two horizontal arrows represent the polymerization of two mixtures of slightly different initial composition. The diagram shows that the extent of polymerization at which phase separation starts is very sensitive to the initial monomer or LC concentration.

4.2. *Morphology and conversion phase diagram*

The most intriguing results from the three series of experiments summarized in table 1 are the absence of coalescence for LC concentrations of less than 81 wt % (except sample 6) and the abrupt change of the shape of the LC domains as a function of initial LC content and curing temperature.

The absence of coalescence points to liquid–gel separation and the formation of non-spherical domains reflects the inhomogeneous structure of the polymer network. The same phenomena have already been noticed in a simple model system composed of K15/TEGDA [9]. However, in the technical system, the change from spherical to non-spherical occurs within only a one per cent LC concentration range or within a 5 degrees change in the curing temperature. As indicated in the conversion phase diagram of figure 11, the extent of polymerization α at which phase separation starts is very sensitive to the initial LC concentration. The higher the LC concentration, the lower is the conversion at the onset of the phase separation. This was experimentally confirmed by the photo-DSC/turbidity measurements (table 2). This means that the polymerization of two mixtures of slightly different initial LC concentration will lead to a difference of the networks at the onset of the phase separation: either a large volume fraction of a densely and inhomogeneously crosslinked network (for low LC concentrations) which has a sufficiently high elasticity to deform the shape of the LC domains, or a much smaller volume fraction of a loosely crosslinked gel (for high LC concentrations) with a low elasticity and a high flexibility. In the latter case, the droplets remain spherical. In this way the simple diagram explains the various morphologies of the LC domains observed during photopolymerization, as collected in table 1.

In all cases, isolated nematic droplets appear at the beginning of phase separation (cf. figures 3–6). Depending on the experimental conditions, coalescence does or does not occur later in the reaction. If the exposure is continued after the onset of phase separation, a spaghetti-like structure is formed in most cases. We were unable to establish whether or not co-continuous phases result at the end of the reaction. However, the relatively high LC contents used might favour the formation of a continuous LC phase.

At high LC contents (samples 1–3), considerable coalescence occurs. This indicates that the gel is either very weakly crosslinked or that gelation occurs after phase separation, i.e. liquid–liquid demixing of a polymer rich and an LC rich phase precedes gelation. At medium LC contents, very few or no coalescence events are observed; phase separation occurs at higher conversion and the gel is strong enough to prevent coalescence. In sample 4 most of the droplets remain separated. This situation is depicted schematically in figure 12 (*a*).

In sample 5, the phase separation occurs still later in the reaction so that the gel is strong enough to prevent coalescence of LC droplets. Moreover, its elasticity and inhomogeneity are also high enough to deform the LC domains. Therefore, a non-spherical morphology results (figure 12 (*b*)). In samples 7 and 8, the LC domains are even more influenced by the presence of the gel and hence they remain very small (figure 12 (*c*)). At low LC content the gel is so strong at phase separation that the domains become vanishingly small.

The distorting effect of a decreasing LC content on the droplet shape can be offset by lowering the curing temperature: sample 6 shows coalescence. This temperature effect on droplet shape can also be readily understood from the conversion phase diagram. Now the LC content is kept constant, but upon increasing the temperature, the interaction parameters χ_{M-P} and χ_{LC-P} will decrease, leading to an increase of the swelling capacity of the polymer network. Consequently, the phase separation line shifts slightly upwards (figure 13). A higher

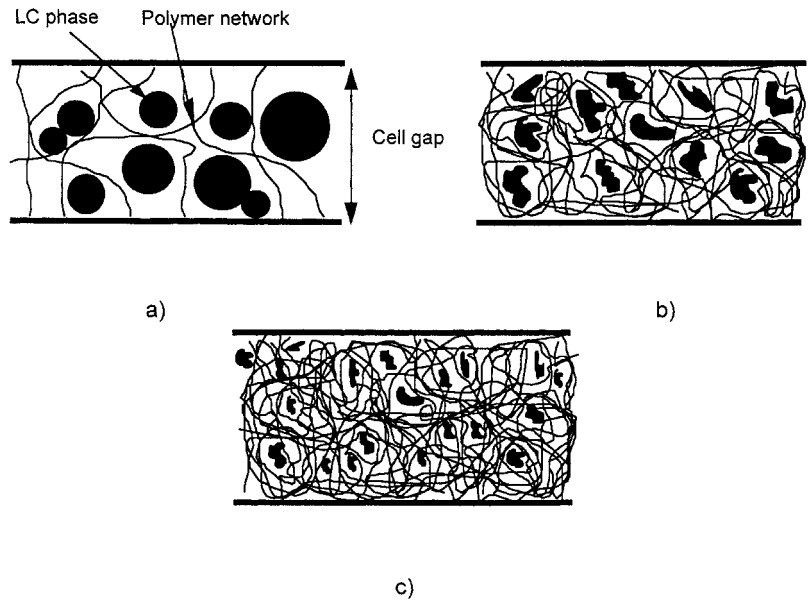

Figure 12. Schematic representation of the gel at the onset of the phase separation. Gel content at incipient phase separation increases from (*a*) to (*c*) (see text for discussion).

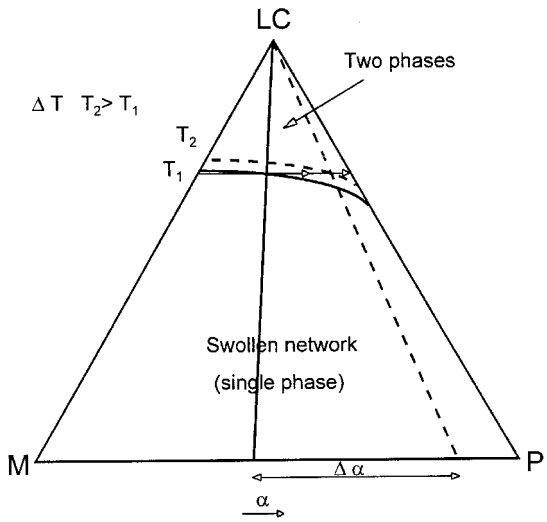

Figure 13. Ternary conversion phase diagram (schematic): effect of the temperature of polymerization on the phase separation process. α = degree of monomer conversion.

curing temperature delays the phase separation significantly, so that at the onset of phase separation, a more densely crosslinked gel is present. Its elasticity is then sufficiently high to deform the shape of the LC droplets (figure 12 (*b*)). Conversely, a low curing temperature leads to early phase separation. Therefore, a partially crosslinked gel is present at the onset of phase separation. The LC droplets can easily deform this gel, so they will keep their spherical shape (figure 12 (*a*)) and eventually show coalescence (sample 6).

Cooling after polymerization decreases the swelling capacity of the network due to an increase of χ_{M-P} and χ_{LC-P}. Consequently, additional LC and monomer molecules separate out. Droplets may grow in size (sample 3), in number, or both (samples 6, 5 and 4), depending on the strength of the gel. During heating, droplets which have been formed during cooling disappear again due to the recovery of the swelling capacity of the polymer network.

The ternary conversion phase diagram also explains why at a low LC content or at a high curing temperature there may be no phase separation at all. At low LC concentrations or high curing temperatures, the phase separation is not only delayed until high conversion, such that only very small droplets can be formed, but also the increasing gel fraction reduces the driving force for phase separation until the swelling capacity of the network is sufficient to accommodate all of the LC molecules.

The absence of coalescence in a large number of experiments is considered strong evidence for liquid–gel separation rather than liquid–liquid demixing. An alternative explanation is a high viscosity. However, in [9] we have shown that even the high viscosity occurring during very late phase separation in a linear polymer/LC system does not suppress coalescence. The presence of a gel at phase separation is even more clearly visible when distorted droplets are formed. This is difficult to visualize in any liquid solution.

In the literature, it is often assumed that phase separation occurs as a result of the increasing size of the growing polymer molecules, i.e. by liquid–liquid demixing [1–4, 13, 14]. This may be correct for linear polymers where the morphology is stabilized by vitrification rather than by crosslinking and also in the first part of crosslinking polymerization through step reactions. In

the latter case, according to Doane [2], the solubility of the LC decreases due to the decreasing compatibility of the growing polymer chains with the LC solvent; isotropic droplets containing LC and monomer separate and grow until gelation of the polymer matrix arrests further growth. Then purification of the droplets occurs by consumption of their dissolved monomer by the still growing matrix. In step reactions, demixing will precede gelation since gelation generally occurs at relatively high conversion (33–75 wt %) [15]. However, one would expect a different order of events if PDLCs are obtained through radical chain crosslinking reactions as described in the present paper. Chain polymerization involves the immediate formation of very high molecular weight polymer upon starting the reaction. If the reaction mixture contains a significant fraction of a multifunctional acrylate, as PN393 does, gelation may occur almost at the beginning of the reaction, often at conversions of less than 1 wt % and usually without phase separation. Therefore, the driving force for phase separation is crosslinking rather than size inequality between polymer and LC molecules. In samples polymerized at high dilution or low temperature which do show coalescence, the situation is less clear. Liquid–gel separation followed by strong deformation of the loose gel is still possible, but so is liquid–liquid demixing.

The TL205/PN393 system has recently been studied by Srinivasarao and Amundson [16]. These authors also observed coalescence at high LC content (82·4 wt %) and no coalescence at a slightly lower LC content (80 wt %) at 26°C. They did not report an abrupt change from spherical to non-spherical droplets upon reducing the LC content, and the developments of morphology at 80 and 75 wt % LC were similar, albeit that at 75 wt % LC, smaller droplets were formed. We also found that droplet size decreases with decreasing LC content (table 1). It should be noted that the light intensity used in [16] was much higher than in the present paper.

4.3. *Morphology at phase separation and contrast ratio*

The data in figure 9 show that the contrast ratio passes through a pronounced maximum upon reduction of the LC content from 82 to 78 wt %. The steepest increase occurs simultaneously with a change in the shape of the LC droplets from spherical to non-spherical. The slow decline on further reduction of the LC content can be explained by a late phase separation leading to domain sizes which are much smaller than the wavelength of the light and therefore do not scatter the incident light efficiently (see figure 6). Variation of the curing temperature produces a similar result (figure 10). Here too, the decline beyond the maximum can be explained by a later phase separation, leading to very small LC domains (cf. figures 12 (*b*) and 12 (*c*)).

The question remains why the non-spherical LC domains lead to a much better contrast ratio than the spherical ones. It looks as if at 25°C and at 80 wt % of TL205, the network elasticity at the onset of the phase separation is exactly that required to achieve the proper size of the LC domains for optimal scattering (typical sizes are around 1–2 μm). However, from figures 3 and 4 it can be seen that the actual domain sizes are much larger than 1 μm and therefore much larger than the wavelength of visible light. Such a PDLC should exhibit a poor contrast ratio. At the onset of the phase separation, the gel must have just enough elasticity to avoid coalescence of LC droplets and to prevent excessive growth of the LC domains by diffusion. Since at incipient phase separation, the LC domains still contain monomers and a photoinitiator, subsequent UV exposure will initiate secondary phase separation. This process is well documented [12, 16–18]. It might lead to LC domains with an adequate size for efficient scattering of light. It could also be that splitting of relatively large domains into smaller ones leads to different LC orientations in the sub-domains, such that multiple scattering is enhanced. So far, we believe that the contrast ratio of a PDLC is controlled by the elasticity of the gel at phase separation and by the degree of secondary phase separation. Although the appearance of the samples changes considerably during further exposure, the localization of the transition between spherical and non-spherical LC domains appears to be a valuable guideline to determine the right LC content and curing temperature for optimal scattering. However, the questions of precise domain structures and LC phase continuity in the fully cured samples require further study.

4.4. *Morphology and reaction mechanism*

Morphology is known to be a key parameter. Yamagishi *et al.* claim that the reaction mechanism of polymerization (step or chain reaction) plays a dominant role with respect to morphology and performance [19, 20]. A 'polymer ball' morphology was associated with a chain reaction, whereas a more desirable 'Swiss cheese' morphology should result from a step reaction or from a chain reaction with excessive chain transfer, such as the thiol-ene system present in NOA65 [20]. Unfortunately, it is not possible to change the mechanism only, without changing molecular interaction parameters at the same time.

Our experiments show that widely different morphologies can be obtained without any change of the mechanism. Both in TL205/PN393 and K15/TEGDA, the crosslink density of the gel at the onset of phase separation dominates the morphology of the LC droplets. Similarly, the differences in electro-optic performance which have been observed with polymer ball and Swiss

cheese systems might well be due to differences in gel point and monomer conversion at the onset of the phase separation.

5. Conclusions

The isothermal phase separation during chain crosslinking polymerization of PN393/TL205 is driven by liquid–gel demixing rather than by liquid–liquid demixing if the polymerization is carried out at 25°C and if the LC content does not exceed 80 wt %. The abrupt change from spherical to non-spherical droplet shapes upon lowering the LC content or increasing the temperature of reaction reflects the inhomogeneity of the densely crosslinked gel. At the morphological transition from spherical to non-spherical, the contrast ratio passes through a maximum. The increase is speculatively ascribed to favourable secondary phase separation, and the decrease to an observed reduction in droplet size. The influence of variation of LC content and temperature of reaction on the shape of the droplets has been explained qualitatively by means of a conversion-phase diagram calculated on the basis of the Flory–Huggins–Dušek theory.

C. S. thanks the EU for financial support of this work under contract ERB4001GT930175.

References

[1] Drzaic, P. S., 1995, *Liquid Crystal Dispersions*, (Singapore: World Scientific).
[2] Doane, J. W., 1990, *Liquid Crystals: Applications and Uses*, edited by B. Bahadur, (Singapore: World Scientific), p. 361.
[3] Doane, J. W., Golemme, A., West, J. L., Whitehead, J. R., and Wu, B. G., 1988, *Mol. Cryst. liq. Cryst.*, **165,** 511.
[4] Montgomery, G. P., Smith, G. W., and Vaz, N. A., 1994, *Liquid Crystalline and Mesomorphic Polymers*, edited by V. P. Shibaev and L. Lam, (New York: Springer), p. 149.
[5] Lovinger, A. J., Amundson, K. R., and Davis, D. D., 1994, *Chem. Mater.*, **6,** 1726.
[6] Nazarenko, V. G., Sarala, S., and Madhusudana, N. V., 1994, *Jpn. J. appl. Phys.*, **33,** 2641.
[7] Lackner, A. M., Margerum, J. D., Ramos, E., and Lim, K.-C., 1989, *Proc. SPIE*, **1080,** 53.
[8] Margerum, J. D., Lackner, A. M., Erdmann, J. H., and Sherman, E., 1991, *Proc. SPIE*, **1455,** 27.
[9] Serbutoviez, C., Kloosterboer, J. G., Boots, H. M. J., and Touwslager, F. J., *Macromolecules* , (in press).
[10] Boots, H. M. J., Kloosterboer, J. G., Serbutoviez, C., and Touwslager, F. J., *Macromolecules* , (in press).
[11] Kloosterboer, H., Serbutoviez, C., Boots, H., and Touwslager, F., 1996, *Polym. Mater. Sci. Eng.*, **74,** 190.
[12] Kloosterboer, J. G., Serbutoviez, C., Boots, H. M. J., and Touwslager, F. J., *Polym. Commun.*, (in press).
[13] Smith, G. W., 1993, *Int. J. mod. Phys. B.*, **7**, 4187.
[14] (*a*) Hirai, Y., Niiyama, S., Kumai, H., and Gunjima, T., 1990, *Proc. SPIE*, **1257,** 2; (*b*) *idem*, *Reps. Res. Lab. Asahi Glass Co.* 1990, **40,** 285.
[15] Flory, P. J., *Principles of Polymer Chemistry*, 1953, (Ithaca NY: Cornell University Press), p. 348.
[16] Srinivasarao, M., and Amundson, K., 1996, *Polym. Prep.*, **37**(1), 200.
[17] Kim, J. Y., Cho, C. H., Palffy-Muhoray, P., Mustafa, M., and Kyu, T., 1993, *Phys. Rev. Lett.* **71,** 2232.
[18] Shen, C., and Kyu, T., 1995, *J. chem. Phys.*, **102,** 556.
[19] Yamagishi, F. G., Miller, L. J., and Van Ast, C. I., 1989, *Proc. SPIE*, **1080,** 24.
[20] Vaz, N. A., 1989, *Proc. SPIE*, **1080,** 2.